EFDA–JET–PR(07)17

A. Nicolai,U. Daybelge, M. Lehnen, M.Z. Tokar, B. Unterberg, C. Yarim
and JET EFDA contributors

Interaction of Plasma Rotation and Resonant Magnetic Perturbation Fields in Tokamak

Interaction of Plasma Rotation and Resonant Magnetic Perturbation Fields in Tokamak

A. Nicolai[1], U. Daybelge[2], M. Lehnen, M.Z. Tokar[1], B. Unterberg[1], C.Yarim[2] and JET EFDA contributors*

JET-EFDA, Culham Science Centre, OX14 3DB, Abingdon, UK

[1]Institut Jülich GmbH, Euratom für Plasmaphysik, Forschungszentrum Jülich GmbH, EURATOM Association, Trilateral Euregio Cluster, D-52425 Jülich, Germany
[2]Istanbul Technical University, Faculty of Aeronautics and Astronautics, 80626 Maslak, Istanbul, Turkey
** See annex of M.L. Watkins et al, "Overview of JET Results ", (Proc. 21st IAEA Fusion Energy Conference, Chengdu, China (2006)).*

Preprint of Paper to be submitted for publication in Nuclear Fusion

ABSTRACT.

The interaction between plasma rotation and perturbation fields is described by the ambipolarity constraint and the parallel momentum balance, both emanating from the revisited neoclassical theory, and the electrodynamical screening of the resonant perturbation field at the singular surfaces. This screening depends mainly on the slip between the rotating plasma and the resonant field. The neoclassical theory, valid in the collision dominated regime and accounting for gyro viscosity includes arbitrary plasma cross -sections, anomalous viscosity, ponderomotive forces,Neutral Beam Injection (NBI), pressure anisotropization and a momentum source due to ergodicity which has a considerable impact on the plasma rotation as demonstrated in TEXTOR.

To estimate the influence of the perturbation coils on the plasma rotation, the radial magnetic field (proportional to the helical flux function) are Fourier analyzed (using 'intrinsic' coordinates) and the total field is used for field line tracing thus obtaining the ponderomotive momentum input and the extension Δ_e of the ergodic layer at the edge. Both procedures account for the full plasma geometry. Δ_e is assumed to be independent from the rotational state because of the boundary condition Vt=0. In a second step the obtained velocity profiles are used to compute the screening at the singular layers and thus the reduction of the island width due to plasma rotation.

The mainresults canbe summarized asfollows: Using in the case of the TEXTOR Pulse No: 94092 the diffusion coefficient $D_M = 2\ 10^{-6}$ m (typical for the 12/4 configuration) the observed increase of vt by $\Delta v_t \approx$ 5km/sec can be sec reproduced. Inside the plasma the slip prevents any influence of the ponderomotive forces, thus yielding a constant increase of the $v_t(r)$ - *profile* by Δv_t.

Assuming in the case of the error field correction coils (n=1) of JET the current I_{hel} = 30kA and using for the plasma background the data of Pulse No: 67951 in the static case an ergodized layer (Δ_e(n=1) ≈ 20cm in the vicinity of the unperturbed x -point) and large m=2, m=3 (n=1) islands ($W_{m=2,n=1}$ =10cm) are obtained whereas in the n=2 configuration the analogous parameters are ≈ Δ_e(n=2) 18cm and W_m = 4cm i.e. Δestays roughly the same and the island width is strongly reduced thus indicating the superiority of this configuration. Plasma rotation (v_{tmax} = 180km/sec) reduces the width Wmto small value. (However, tearing mode physics which may lead to mode locking is not included in this consideration).

1. INTRODUCTION

The interaction between the poloidal or toroidal spin-up [1]-[35] and the perturbation fields, is an important issue for fusion oriented devices and is therefore under investigation experimentally and theoretically. The importance of the perturbation coils [26]-[45]is underlined by the fact, that they are considered as a means to mitigate the ELMs.

The revisited neoclassical theory [2]-[6] which is essentially based on Braginskii's equations [7]-[8], allows within the framework of a rigorous analytical approach the calculation of the two dimensional velocity field on the flux surfaces and the perpendicular ambipolar electric field, i.e. the quantities which determine the electrodynamical screening and which are believed to be important

for the L-H transition. This theory is valid in collision dominated plasmas with steep gradients and was able to reproduce the toroidal spin up in the divertor tokamak ALCATOR C-MOD [4], [5], [24].

Since the momentum input due to helical coils and due to the beam have a strong impact on the velocity field, in [11] and [12] the respective source terms due to the 'ponderomotive forces' [14] and the forces due to pressure anisotropization [10] were included in the neoclassical momentum balances. Depending on the island overlap the helical perturbations can act as means for ergodizing the magnetic field in particular in the vicinity of the separatrix and thus for the 'ergodic' momentum source at the plasma edge [13].

The neoclassical equations were modified to account for anomalous viscosity as well [11].

In the H -mode the region of the high confinement is -as in ALCATOR [12] -restricted to the edge region where a temperature pedestal is build up due to the steep velocity profile (thus due to a large velocity shear). However, the large pressure gradient in the pedestal region in general exceeds the ballooning-peeling limit and thus gives rise to the edge localized modes (Type I ELMs) which are supposed to be dangerous for the divertor plate. Therefore at DIIID the use of perturbation coils ('I -coils, C -coils') were under investigation and it was demonstrated that in wide range of plasma parameters ELM suppression was achieved [43]. Although precise mechanism for this is still under investigation, the additional parallel transport due to ergodization of edge region at the separatrix [26] is considered as the main reason for the ELM suppression. In this context the reduction of the normalized pressure gradient may lead to ELM -stabilization.

This underlines the importance of the width Δe of the ergodic layer at the separatrix.

An important obstacle in the application of the perturbation coils could be the excitation of islands in the bulk plasma and thus evoking disruptions. Therefore the screening of the perturbation field due to plasma rotation at a high slip -frequency is considered by applying the aforementioned model in which the source term due to the ponderomotive forces acounts for screening and breaking. Thus the impact of rotation on the island width can be assessed.

The paper is organized as follows: In section (2) the basic equations of the revisited neoclassical theory are summarized and the characteristic quantities are given. In section (3) the electromagnetic screening and in section (4) the source terms for a self consistent model are discussed. A short summary of the treatment of the magnetic field structure by Fourier analysis and field line tracing is given in section (5). Finally, after some remarks about the geometry of the perturbation coils [section (6)], results concerning more recent shots at TEXTOR and JET are presented in section (7).

2. AMBIPOLARITYCONSTRAINTANDPARALLELMOMENTUMBALANCE

As mentioned already, the revisited neoclassical theory accounts in particular for steep temperature and density gradients at high collisionality. Since it is a collision dominated theory, it is based on the fluid equations for particle, momentum and energy conservation [2]-[6]. For a two-component plasma with the velocities $\vec{u}_j$, the densities nj,the particle sources $\vec{S}_j(x, t)$, the friction forces $\vec{R}_j(x, t)$ and the momentum input $\vec{S}_j^M(\vec{x}, t)$ (j=e,i) we get as momentum conservation equation

$$m_j n_j \frac{d\vec{u}_j}{dt} = -\nabla P_j - \nabla \cdot \vec{\vec{\Pi}}_j - eZ_j n_j(\vec{E} + \vec{u}_j \times \vec{B}) - \vec{R}_j + \vec{S}_j^M \quad (1)$$

P_j, $\vec{E}$ and $\vec{B}$ are the scalar pressure, the electric and magnetic field, respectively. We project equation (1) in the toroidal direction and account for inertia, parallel, perpendicular and gyro-viscosity [7]-[8], average over a flux surface, impose the ambipolarity constraint and get for the poloidally averaged toroidal velocity u_ϕ [11]

$$\frac{1}{r}\frac{\partial}{\partial r}\left[r\eta_2\left(\frac{\partial u_\phi}{\partial r} - M_1 \frac{0.107q^2}{1+\frac{Q^2}{S^2}}\frac{\partial ln\, T}{\partial r}\frac{B_\phi}{B_\theta}u_\theta\right)\right]$$
$$= m_i n_i \left(\frac{\partial}{\partial t} + \nu_{cx}\right) u_\phi + T_{NBI} + T_{ANI} + T_{j\times B} + T_{ergo_t} \quad (2)$$

u_θ is the averaged poloidal speed, η_2 is the perpendicular viscosity coefficient. The radial coordinate r is the effective radius $r = \sqrt{\frac{V(\psi)}{2p^2 R}}$ $V(\psi)$ is the volume of the flux surface ψ. M1 is a metric quantity of the order unity accounting for elongated cross -sections [11]. In the case of a circular cross -section we get $M_1 = 1$ analytically. [2]. For elongated cross -sections M_1 can be evaluated numerically. For a JET -plasma with an elongation $k = 1.7$ we get $M_1 = 0.95$, i.e. close to unity, mainly due the definition of the effective radius. We note that using the minor Å„ half axis of a flux surface as radial coordinate would increase M_1 by $\sqrt{k}$ [11].

We note that as in [11] the classical viscosity must be replaced by an anomalous one to reproduce TEXTOR -or JET -data. Here the growth rate of the ITG -instability (Ion Temperature Gradient -instability) was used to define the diffusivity for the momentum transport in analogy to the energy transport. The velocities Q and S are defined by [4], [11]

$$Q = [4u_\theta - 5\nu_n(1 + \frac{1}{2\eta})]\frac{B_\phi}{B} \quad (3)$$

and

$$S = \frac{8\nu_n \eta}{\Lambda}\frac{B_\phi}{B} \quad (4)$$

with the velocity $\nu_n = \frac{T}{eB}\frac{\delta ln(n)}{\delta r}$ and the well known ratio

$$\eta = \frac{\frac{\partial ln(T)}{\partial r}}{\frac{\partial ln(n)}{\partial r}} \quad (5)$$

The important quantity $\Lambda = \frac{\nu_i}{\Omega_i}\frac{q^2R^2}{L_T r}$ acts as a switch for the finite Larmorradius effects. For large gradient lengths L_T the neoclassical result is retrieved, i. e. $\frac{Q}{S}$ is becoming small. The charge exchange reactions are characterized by the charge exchange frequency $\nu_{cx} = <\sigma v>_{cx} n_0$. $<\sigma v>_{cx}$ is

the rate coefficient for charge exchange, and n_0 the neutral gas density. The source terms T_{NBI}, $T_{AN\,I}$, $T_{j\times B}$,T_{ergo_t} account for NBI, pressure anisotropization due to helical perturbations, for the $\vec{j}\times\vec{B}$ - force at the singular surfaces and for the averaged radial current in the ergodized region [39], [41].

We define the dimensionless quantities $g = \frac{u_\phi}{v_T}$, $h = \frac{u_\theta}{v_T}$ *and* $x = \frac{r\text{-}r_{in}}{L_\psi}$.

Here we used the (constant, positive) velocity $v_T = \frac{1}{eB_\phi}\frac{T_{in}}{L_\psi}$. T_{in} is the temperature at the point P_{in} with radius rin and the length $L_\psi = L_T(r_{in})$ is L_T at P_{in}. In the case of ALCATOR C-MOD [4] Pin is the 'inflection' point which is defined as the locus of vanishing curvature of the ion temperature pedestal. In the case of TEXTOR (without temperature pedestal) P_{in} is assumed to coincide with the plasma edge (i. e. $r_{in} = r_{max}$, r_{max} is the minor plasma radius). The length $L_\psi = L_T(r_{in})$ is $L_T(\frac{\delta ln\ T}{\delta r})$ at P_{in}.With $G = \frac{\delta g}{\delta x}\frac{0.107q^2}{1+\frac{Q^2}{S^2}}\frac{\delta lnT}{\delta x}\frac{B_\phi}{B_\theta}\ h$ and $x' = x + \frac{r\text{-}r_{in}}{L_\psi}$ we get the dimensionless equation (by multiplying with $\frac{t_c}{n_i m_i v_T}$ where $t_c = \frac{n_i m_i L_\psi{}^2}{\eta_2(r_{in})}$ is the characteristic time [11])

$$\frac{1}{x'}\frac{1}{\eta_2}\frac{\partial}{\partial x}\ [x'\eta_2 G] = \hat{T}_{CX} + \hat{T}_{NBI} + \hat{T}_{ANI} + \hat{T}_{j\times B} + \hat{T}_{ergo_t} \tag{6}$$

Taking the parallel components of the terms in the momentum equation 1 and accounting in particular for the gyro-viscosity tensor [4] we get a nonlinear relation between the poloidal and toroidal plasma velocities [4] in the case of large aspect ratio and circular cross -section.

$$\begin{aligned}(h^* + 1.833)\,M_1 = \frac{0.45\Lambda}{1+\frac{Q^2}{S^2}}\{&\frac{0.107q^2}{1+\frac{Q^2}{S^2}}\,h^* + \frac{1}{2}\,\frac{1}{[\frac{\partial\hat{T}}{\partial x}]^2}\,(g^*)^2 \\ -\frac{1}{\frac{\partial\hat{T}}{\partial x}}&g^*[h^* - (1+\frac{2}{\eta})] + 1.9[h^* - 0.8(1+\frac{1.6}{\eta})]^2\} + \hat{T}_{ergo_p}\end{aligned} \tag{7}$$

Here the definitions $g^* = \frac{B_\theta}{B_\phi}\frac{u_\theta}{\eta v_n}$, and $h^* = \frac{u_\theta}{\eta v_n}$ are used, to cast equation (7) in a convenient form. $\hat{T}_{ergo_p}$ accounts for momentum input by the averaged radial current due to ergodization.

3. SCREENING OF HELICAL PERTURBATION FIELDS.

In general the plasma rotates at a speed different from that of the perturbing field. Therefore the slip frequency ω (like in an induction motor) must be accounted for [14]. This frequency is defined as $\omega = \omega_p - \omega_f$. ω_p is the plasma rotation frequency $\omega_p = m\Omega_{\theta,p} - n\Omega_{\phi,p}$ and ω_f the helical field rotation frequency $\omega_f = m\Omega_{\theta,f} - n\Omega_{\phi,f}$ .m, n are the poloidal and toroidal mode numbers, respectively. $\Omega_{\theta,p}$, $\Omega_{\theta,f}$,$\Omega_{\theta,p}$, $\Omega_{\theta,f}$ are the poloidal rotation frequency of the plasma, the poloidal rotation frequency of the helical field, the toroidal rotation frequency of the plasma and the toroidal rotation frequency of the helical field, respectively. If the slip frequency is very large, no momentum transfer to the singular surface can be expected because of the eddy currents which prevent the penetration of the helical field. At low slip frequencies the eddy currents are small enough to allow the field to penetrate.

Outside the singular layer ideal MHD can be applied and the equilibrium condition under the influence of the helical field

$$\psi = \psi(r) exp[i(m\theta - n\phi + \omega_f t)] \tag{8}$$

is given by the 'ideal tearing mode equation' [14].

$$\frac{1}{r}\frac{d}{dr}(r\frac{d\psi}{dr}) - \frac{m^2}{r^2}\psi - \frac{\mu_0 m \frac{dj}{dr}}{B_\theta(m - nq)}\psi = 0 \tag{9}$$

j(r) is the plasma current density which is asumed to be parabolic in r, B_θ is the corresponding poloidal field. Equation (9) allows to compute 'tearing mode stability index'

$$\Delta' = \left[r \frac{d\psi_{plasma}}{dr} \right]_{r_{s-}}^{r_{s+}} \tag{10}$$

We assume here $\Delta' < 0$ so that the plasma is tearing mode stable [11]. Otherwise the tearing mode physics would invalidate the subsequent considerations. According to the considerations in [14] at the singular surface the plasma acts roughly like the rigid armature of an induction motor because viscosity and inertia prevent the large displacement of the plasma correlated to the large changes of the magnetic field due to equation (9). The dependence of the flux function ψ_s in the singular layer with the width δ_s can then inferred from Ampere's and Faraday's law. The first one relates the current density j_s to the jump of the magnetic field across the layer

$$\mu_0 j_s = \frac{1}{\partial_s r_s}\left[r\frac{d\psi}{dr} \right]_{r_{s-}}^{r_{s+}} = \frac{1}{\partial_s r_s}(\Delta'\psi_s + 2m\psi_v) \tag{11}$$

ψ_v is the flux function of the vacuum field of the perturbation coils at r=rs. On the other hand Ohm's law connects the current density with the electric field generated by the oscillating magnetic field in the singular layer with the electrical conductivity σ_s

$$\mu_0 j_s = \mu_0 E\sigma_s = \mu_0\psi_s\sigma_s = i\mu_0\omega\psi_s\sigma_s \tag{12}$$

For ψ_s one gets in this ('rigid armature') approximation

$$\psi_s = \psi_v \frac{2m}{-\Delta' + i\omega\tau_s} \tag{13}$$

With

$$\tau_s = \upsilon_0 \sigma r_s \delta_s$$

The width of the layer can be estimated as [14]

$$\delta_s = r_s \left[\frac{\tau_h^2}{\tau_R \tau_V}\right]^{\frac{1}{6}} \tag{14}$$

Here the hydrodynamic time is

$$\tau_h = \frac{R_0}{r_s n_s s}\tau_a \tag{15}$$

τ_a is the Alfvén -time

$$\tau_a = \frac{r_s}{v_a} = \frac{r_s}{\sqrt{\frac{B_0^2}{n_s m_i \mu_0}}} = r_s\sqrt{\frac{n_s m_i \mu_0}{B_0^2}} \tag{16}$$

n_s is the ion density at the singular layer. The shear parameter s is defined by

$$s = \frac{rq'}{q} \tag{17}$$

The viscous diffusion time can be expressed as

$$\tau_V = \frac{r_s^2 m_i n_s}{\eta_2(r_s)} \tag{18}$$

Finally, the resistive time is

$$\tau_R = \mu_0 r_s^2 \sigma(r_s) \tag{19}$$

Accounting for the layer physics in the 'visco -resistive' regime [14], [15] in which the plasma inertia is neglected, we get for the characteristic time τ_s

$$\tau_s = \tau_{VR} = 2.104\,\frac{r_s}{\delta_s}\left(\frac{\tau_R}{\tau_V}\right)^{\frac{1}{3}}\tau_H^{\frac{2}{3}}\tau_R^{\frac{1}{3}} f_{geo} \tag{20}$$

with $f_{geo} = 1$ in [15] However, more recently, in [28] and [27]. $f_{geo} = (1 + 2q^2)^{1/3}$ was introduced. In contrast to [15] this factor accounts for the inertia [45] in the layer equation.

Real and imaginary part of expression (13) allow e. g. to compute the phase shift between ψ_s and ψ_f. For static fields the phase shift vanishes and $\psi_s = \psi_v \frac{2m}{-\Delta'}$ is in general larger than ψ_v ('amplification'). At high slip frequencies, beyond the critical frequency

the flux function in the singular layer is considerably lower than ψ_v .

Since $\frac{\delta_s}{2mr_s} = (\frac{\tau_H}{\tau_V})^{1/6} (\frac{\tau_H}{\tau_R})^{1/6} \frac{1}{2m} = f_\tau$ depends only very weekly on the plasma parameters, it follows from equation (13) that the 'screened' Fourier component is given by

$$B^s_{m,n} = B^v_{m.n} \frac{1}{\sqrt{\alpha^2 + (\omega \tau_{VR} f_\tau)^2}} \tag{21}$$

with $\alpha = \frac{-\Delta'}{2m}$ which is of order unity since in [11] the estimate $\Delta' \approx 5$ was obtained.

4. MOMENTUM SOURCES

The analytic expressions for the momentum sources mentioned already before are given and discussed here.

4.1.THE ROLE OF RADIAL CURRENTS DUE TO FIELD LINES TO CHASTIZATION

The electric currents under the condition of magnetic field line stochastization originate from the radial excursion of the field lines under the influence of the radial field of perturbation coils. Due to the generalized version of Ohm's law the current density parallel to the field lines is given by

$$j_{||} = \sigma_{||} \vec{b} \cdot [-\nabla \Phi + \frac{T_e}{e} (\nabla ln\, n + 1.71 \nabla ln\, T_e)] \tag{22}$$

Replacing the parallel derivative according to $\vec{b} \cdot \nabla \sin(\alpha) \frac{d}{dr}$ by the dr radial derivative (where α is the angle between the field line and the toroidal direction). We get

$$j_{||} = \sigma_{||} [-\frac{d}{dr} \Phi + \frac{T_e}{e} (\frac{d}{dr} ln\, n + 1.71 \frac{d}{dr} ln\, T_e)] sin(\alpha) \tag{23}$$

Projecting the obtained current in the radial direction and averaging over the unperturbed flux surfaces [41] we obtain the radial current due to ergodization.

$$< j_{||,r} >= \sigma_{||} < sin^2(\alpha) > [E_r - \frac{T_e}{e} (L_n^{-1} + 1.71 L_T^{-1})] \tag{24}$$

$L_n = -dr/d \ln n$ and $L_T = -dr/d \ln T$ are the e-folding lengths of plasma density and electron temperature of the prescribed plasma background. Here it is assumed that $< j_{||,r} >$ is a perturbation which does not perturb the magnetic field of the background plasma, i. e. a low beta approximation is made where the magnetic field is large enough.

Since the mean squared displacement perpendicular to the unperturbed field lines after moving by the distance $\tilde{L}_k$ in the toroidal direction is $D_M \tilde{L}_k$ (D_M is the field line diffusion coefficient and $\tilde{L}_k$ the (somewhat modified) Kolmogorov length) we get the estimate $<sin^2(\alpha) > = \frac{D_{FL}}{\tilde{L}_K}$.

A more refined analysis can be found in [41]. Because of ambipolarity the radial current density (24) must be compensated by the averaged radial component of the perpendicular current density $<j_{\perp,r}>$:

$$< j_{\perp,r} > + < j_{/\!/,r} > = 0$$

The unperturbed perpendicular current density and the ambipolarity constraint to be imposed on this current density, was considered in section 2. The additional toroidal momentum input is given by the Lorentz force density

$$T_{ergo_t} = B_\theta < j_{\perp,r} >$$

Analogously we have for the poloidal momentum input

$$T_{ergo_p} = B_\phi < j_{\perp,r} >$$

The respective dimensionless source terms are $\hat{T}_{ergo_t} = \frac{B_\phi < j_{\perp,r} >}{n_{in} M_i \nu_T \eta_2}$ and $T_{ergo_t} = -\frac{2}{3} \frac{B_\phi R^2 < j_{\perp,r} >}{\eta_0 \eta \nu_n} \cdot \eta_0$ [3] is the parallel viscosity coefficient.

4.2. NEUTRAL BEAM INJECTION

Due to neutral injection [6] the momentum deposited in a radial volume element $\Delta V = 2\pi R 2\pi r dr$ during the time Δt is [11] $\Delta(m v_i N_i)\Delta V = m\dot{N}_0 \Delta t \frac{dl}{l_{mfp}} v_0$. dl is the line element along the beam path, $v_0 = \sqrt{\frac{E_b}{2m_b}}$ the speed of the neutrals and lmfp the mean free path length due to charge exchange. Using the beam -, the torus -geometry and the charge exchange cross -section we get [11] $\dot{v}_i \frac{m}{sec^2} = \frac{N_0 < \sigma v >_{cx}}{2\pi R_0 2\pi r \sqrt{2} \in \sqrt{\kappa}} 1.68\ 10^7 \frac{P_{MW}}{R_{keV}} \frac{1}{R_0[m]\, r\,[m] \sqrt{\in}}$.

4.3. PRESSURE ANISOTROPIZATION DUE TO THE HELICAL PERTURBATIONS [10]

The helical perturbations modulate the absolute value of the total field $B = B_0(\theta)\,[1 + \Sigma_{m,n}\, b_{m,n}(\theta, \phi)]$. $B_0(\theta) = \sqrt{B_{0,\phi}^2 + B_{0,\theta}^2}$ is the axisymmetric Tokamak field and the $b_{m,n}(\theta, \phi)$ are given by $b_{m,n}(\theta, \phi) = \sqrt{\frac{B_{\theta m,n} + B_{\phi m,n}}{B_{0,\phi}^2 + B_{0,\theta}^2}} \sin(m\theta - n\phi + \phi_{m,n})$. $B\theta_{m,n}$ ($B\phi_{m,n}$) are the Fourier components of the perturbing poloidal (toroidal) field [11] and $\phi_{m,n}$ are the phases. Due to the pressure anisotropization introduced by the modulation we get as braking term $< \vec{e}\phi \cdot \nabla \Pi >= K v\phi$ [20],[32] with [10]

$$K = \frac{\sqrt{\pi} p_i}{v_{T_i} R_0} \sum_{m,n} \frac{(B_{0,\theta} B_{\theta_{m,n}} + B_{0,\phi} B_{\phi_{m,n}})^2}{B_0^4} \frac{n^2 q}{|m - nq|} \qquad (25)$$

This expression is derived for the plateau regime and it is valid in the vicinity of of the rational surface with $q = \frac{m}{n}$. However, at the rational surface itself the Pfirsch -Schlüter regime is entered. In this regime the expression (25) must be modified, thus a singularity does not appear. More details are given in [11].

In analogy to NBI the dimensionless source term due to the braking by helical perturbations is given by $\hat{T}_{br} = t_{ci} \frac{K\hat{n}}{\hat{\eta}2}\, g$

4.4. THE TORQUE DUE TO THE $\vec{J} \times \vec{B}$ FORCES IN THE SINGULAR LAYER

Due to the aforementioned screening the dependence of the momentum density transferred to the singular flux surface, on the slip frequency is given by [14], [11]

$$T^*_{j\times B} = T^*_{EM} = \frac{T_{EM}}{4\pi^2 r r_s \delta_s R_0} = -\frac{8\pi^2 m^3 R_0}{\mu_0 4\pi^2 r r_s \delta_s R_0} \frac{\omega\tau_s}{(-\Delta')^2 + (\omega\tau_s)^2} \; |\Psi_v|^2 \tag{26}$$

in $r_s - \delta_s/2 < r < r_s + \delta_i/2$ and $T^*_{j\times B} = 0$ elsewhere. Ψ_v is the vacuum flux function at the singular surface [14]. For the numerical treatment the discontinuous source term defined by the equation (26) is replaced by a continuous one as in [11].

5. MAGNETIC FIELD STRUCTURE

Fourier analysis of the radial field performed at the singular surfaces provides the input for the preceding rotation model, field line tracing is here the main method to demonstrate the destruction of of the flux surfaces in the vicinity of the x -point.

5.1. FOURIER ANALYSIS OF THE PERTURBING MAGNETIC FIELD

The Fourier sine -coefficients of the radial field B_r are given by

$$B_{mn_s} = \frac{1}{2\pi^2} \int_0^{2\pi} d\theta^* \int_0^{2\pi} d\phi B_r[\theta(\theta^*),\phi] \sin(m\theta^* - n\phi) \tag{27}$$

θ^* is the intrinsic angle with the property that a field line $\theta^* - \theta^*_0 = 1/q\,(\phi - \phi_0)$ becomes a straight line on the specific flux surface [17]. $(\phi^*_0 - \phi^*_0)$ is the starting point.

For large aspect ratios and circular cross-section θ^* and θ almost agree, but, in particular in the vicinity of the separatrix of an elongated plasma, they significantly disagree.

A formula analogous to (27) holds for the cosine -coefficients B_{mn_c} .In the following the geometrical sum

$$B_{mn} = \sqrt{B_{mn_s}{}^2 + B_{mn_c}{}^2} \tag{28}$$

of both is envisioned because this sum is decisive for the island width and is almost independent from the phase $\phi_{m,n} = \text{arc tg}\left(\frac{B_{mn_c}}{B_{mn_s}}\right)$. 100 gridpoints were chosen in the toroidal and in the poloidal directions, respectively. Since the coil configuration envisaged in the following mainly have a periodicity in ϕ and not in θ^*, the Fourier decomposition

$$\bar{B}_{n_s}(r,\theta^*) = \frac{1}{2\pi} \int_0^{2\pi} d\phi B_r[\theta(\theta^*),\phi) \sin n\phi \tag{29}$$

is envisaged as well. The coefficients $\bar{B}_{ns}(r, \theta^*)$ depend on the effective radius r and the intrinsic angle θ^*, whereas the coefficients (27) depend on r only.

5.2. FIELD LINE TRACING BY MEANS OF THE GOURDON CODE [31]

To investigate the edge region under the influence of the perturbation coils, the island structure and the ergodic region around the unperturbed separatrix has to be resolved concerning the size and the phase of the (remnant) islands which have a strong poloidal dependenc because of the vicinity of the x -point. Also the structure of the ergodic region around the unperturbed x -point has a significant poloidal dependence. Therefore the edge region is resolved using the (r, θ) -representation mentioned below.

We assume that the equilibrium magnetic field and the radial perturbing field can be superimposed independently. Thus the obtained total magnetic field vector can be used to track the field lines [31]. This presuposes $\Delta' < 0$ and that the slip frequency between the perturbing field and the plasma at the singular surface is small. The field line equations are given by

$$\frac{1}{R}\frac{\partial R}{\partial \phi} = \frac{B_R}{B_\phi} \tag{30}$$

$$\frac{1}{R}\frac{\partial z}{\partial \phi} = \frac{B_z}{B_\phi} \tag{31}$$

R, z, ϕ are cylindrical coordinates. The cylinder axis is the symmetry -axis of the plasma equilibrium [36]. The magnetic field of the nonaxisymmetric conductors is computed by means of BIOT-SAVART's law.

This field is stored on a spatial mesh set up in the R, z, ϕ domain which the field lines are expected not to leave. The field needed during field linetracing is computed by interpolating within the mesh. For the Poincaré -plot two representations by means of different coordinate systems are used to store the intersection points with the plane ϕ = const.[17]:

1. Cylindrical coordinates R, z around the axis of symmetry and
2. Toroidal coordinates (polar coordinates around the magnetic axis). The toroidal coordinates (r, θ) are defined by

$$r = \sqrt{(R - R_0)^2 + z^2} \tag{32}$$

and

$$\theta = arctan\frac{z}{R - R_0} \tag{33}$$

R_0 is the radius of the magnetic axis. Cartesean coordinates $y_{mag} = L_y \frac{r}{a}$ and $x_{mag} = L_x \frac{\theta}{2\pi}$ are used to enhance the visibility of the island structures. L_x and L_y are the lengths of the x -and y -axis. The first representation gives a realistic view of the island shape and size, the second enhances the visibility of the island structures, in particular at the plasma edge, but distorts the islands at the plasma center.

In the examples given below 600 turns per initial point had been chosen so that the number of intersection points with the plane ϕ = 0 is much larger than that of the initial points which are uniformly distributed on a line z = const. between the radii R_{min} and R_{max}. Since the field lines starting at initial points radially in the vicinity of R_{max} reach sometimes the limits of the computational domain, the field line tracing is interrupted giving rise to intersection points which are outside the bulk of the intersection points. These points appearing in Figs.4 -22 have no significance and should be ignored.

6. PERTURBATION COILS

Several conductor configuration had be foreseen, mainly in the vicinity of the plasma edge, at DIIID, TEXTOR and JET. Here we concentrate on the latter two.

6.1. DYNAMIC ERGODIC DIVERTOR AT TEXTOR

The perturbation coils at TEXTOR [11] have the dominant Fourier components in resonance with the q = 3 surface, i. e. the pitch of the conductors corresponds to the (mean) field line pitch at the q = 3 surface. To control the penetration depth, the winding can be switched as mixture of a (m = 12, n = 4), (m = 6, n = 2) and a (m = 3, n = 1) winding. The coil currents are then given by

$$I_j = I_d\,[(1 - p_2 - p_3)\,sin\,(j\,\frac{2\pi}{4} + \omega t) + p_2 sin\,(j\,\frac{2\pi}{8} + \omega t) + p_3 sin\,(j\,\frac{2\pi}{16} + \omega t)]$$

j = 1,...,16. The mixing factors are $p_2 = p_3 = 0$ for the (m = 12, n = 4) –, $p_2 = 1$, $p_3 = 0$ for the (m = 6, n = 2) -and $p_2 = 0$, $p_3 = 1$ for the (m = 3, n = 1) -winding.

6.2. ERROR FELD CORRECTION COILS AT JET

A n = 3 coil system, located on top of the P4 -poloidal field coils, is envisaged at JET to achieve the ergodization of the separatrix region [28]. Available now are the Error Field Correction Coils (EFCCs) [16] producing n = 1 and n = 2 modes for the error field correction. The EFCCs (Fig.7) were implemented at JET to compensate the field errors $\frac{\delta B}{B} \approx 10^{-4}$ and thus to avoid locked modes which may lead to disruptions. Mainly the (m = 2, n = 1), (m = 1, n = 1) (m = 3, n = 1) modes are considered to play a significant role. The EFCCs are mounted at the outer limbs of the yokes. The toroidal extension of one coil is 70o and the shape is approximately that of square with a side length of 6 m. The maximum distance of the conductors from the axis of symmetry is 7m. The maximum current in each coil (with 3 turns) is 48kA, i.e. 16kA per turn. The EFCCs can be configured for n = 1 where two neighboring coils are switched in parallel and the two opposite coils have the opposite current direction (Fig.8). n = 2 can be achieved by choosing current direction to change in neighbouring coils (Fig.9). The EFCCs are supposed to produce Fourier components of the same order as the saddle coils used before [11], i. e. of the order 10^{-4} Tesla.

7. RESULTS

The magnetic fields of the aforementioned coils are analyzed by Fourier decomposition and field line tracing. Depending on the slip frequency between the plasma and perturbing field the islands predicted by field line tracing may be suppressed (large slip) or may be generated as prodicted (low slip) as pointed out in section 3. Furthermore, depending on the sign of Δ' the islands may grow ($\Delta' > 0$) or the 'vacuum' size maystay($\Delta' < 0$).

7.1. TEXTOR

The spectrum of the DED at the q = 2 surface and the possibilities to brake or accelerate the plasma were discussed in [11]. Here we consider the screening and the change of the plasma rotation by an ergodic zone as described insection 4.1.

The main parameters of the investigated shots are T_{imax} = 1.3keV, T_{emax} = 1.63keV, n_{max} = 3×10^{13}cm^{-3}, η =1.6, B_ϕ = 2.23T, $P_{MW_{co}}$ = 0.25MW, $P_{MW_{counter}}$ = 0, plasma current I_p = 300kA, in the case of Pulse No: 94092 and T_{imax} = 2.2keV, T_{emax} = 2.1keV, n_{max} = 3.4×10^{13}cm^{-3}, η =1.6, B_ϕ =2.25T, $P_{MW_{co}}$ = 0.35 MW, $P_{MW_{counter}}$ = 1.3MW, plasma current I_p = 300kA in the case of Pulse No: 97613.

To show the effect of an ergodic layer between r_{e_1} = 40cm and r_{e_2} = 43cm (typical for the 12/4 configuration) field line stochastization with the typical parameters $D_M = 2\times10^{-3}m$ and $\tilde{L}_k$ = 40m is assumed in addition. The gradient lengths of density and temperature in this layer are $L_n = L_T$ = $0.05m$ according to the experimental data of the aforementioned shots. The temperature at the inner rim of ergodic layer is 100eV.

The unperturbed maximum toroidal velocities v_{Tmax} = 40 km (Pulse No: 94092, sec Fig.3 and v_{Tmax} = 140km/sec (Pulse No: 97613, Fig.4 can be reproduced within sec an accuracy of 10%. In the case of Pulse No: 94092 the toroidal velocity increases by ≈ 5km/sec if the ergodic layer (I_{hel} ≈ 6kA)is switched on (Fig.3). To avoid the mode locking, the NBI of Pulse No: 97613 is predominantly in the counter direction. Therefore T_{ergo} (I_{hel} ≈ 20kA) effects a reduction of v_t by Δv_t ≈ 20km/sec (Fig.4). The velocity gradient stays in both cases outside the ergodic layer almost the same, i. e. the ponderomotive forces due to the Fourier components of the 12/4 configuration are negligible. This is confirmed by the screening factor (blue curve in Fig.5). These results agree within the errorbars (≈ 3km/sec) with the experimental findings.

Figure 6 demonstrates the plasma braking at the q = 2 surface for IDED ≥ 2kA. The screening factor outside the q = 2 surface is fs = 1. However, experimentally, a locked mode appears due to the fact that the slip frequency is zero. Therefore the tearing mode physics dominates which is beyond the scope of the considerations here.

7.2. JET

The choice of the JET -data corresponds to Pulse No: 67945 [44] in which the configuration of Fig.8 was used: Major radius R_0 = 296cm, minor half axis a = 85cm, effective radius r_{max} =120cm, plasma current I_p = 1.6MA, toroidal field B_t = 1.84T, NBI = –power P_{NBI} = 18MW, T_{imax} = 7kev,

maximum electron density n_{emax} =4.5×10^{13}cm^{-3} and maximum toroidal speed v_{tmax} = 180km/sec. The configuration of Fig. 9 is treated here as well, however, a comparison with the experimental data was not possible (yet). Figure 10 shows the spectrum for the n = 1 configuration. The (m = 1, n = 1) component is the largest because of the good overlap with sin($\theta^* - \phi$). The (m = 2, n = 1) component is comparable to the (m = 1, n = 3) component and both are around 20% of the just mentioned component because both components have a considerably reduced overlap with the repective sin -function.

Figure 11 shows the analogous spectrum for the n = 2 configuration. The (m = 1, n = 2) component is the largest component, followed by the (m = 2, n = 2) component. From this one can expect that the resonances are far inside and hardly disturb the confinement.

As a reference for the subsequent field line tracing results in Figs.14 (R, Z - representation) and 15 (r, θ - representation) show the unperturbed case, i. e. the assumed equilibrium with KAM - surfaces. A single null plasma with q(r = 0)=0.9 and q_{95} = 4 was chosen. We note that in this case the points marking the field lines are not always uniformly distributed of a specific flux surface. However, this bunching depends on the rationality of q - value of the flux surface and does not mean that the KAM - property is affected.

The results of the Fourier analysis are confirmed by the field line tracing shown in Fig. 16 (n = 1) and 18. As expected, the n = 1 configuration (I_{hel} = 30kA) generates pronounced islands at the q = 2 and q = 3 surfaces (Fig.16). The islands are mainly separated by KAM - surfaces with small islands inserted. The ergodization of the separatrix region is clearly visible; at the x - point (of the unperturbed separatrix) the thickness of the ergodized layer is around 20cm.

The environment of the unperturbed x - point is shown in Fig.17 with a two times higher resolution (the number of the initial points had been doubled). The poloidal range is [230^o – 300^o]. The q = 3 islands near the unperturbed x - point are at their tips toward the x -point somewhat eroded indicating that the ergodization of the x - point region is effective. This is compatible with the fact that in this region no remnant island are visible just in contrast to Fig.19.

The Poincaré plot (Fig.18) generated for the n = 2 configuration with I_{hel} = 30kA is consistent with the spectrum (Fig.11) as well. The (m = 3, n = 2) and (m = 4, n = 2) island chains are visible but the island widths are rather small, corresponding to the small Fourier components. At the x-point (of the unperturbed separatrix) the thickness of the ergodized layer is roughly the same as in the n = 1 case.

The environment of the unperturbed x - point is shown in Fig.19 with a two times higher resolution like in Fig.17. In the ergodic region around the unperturbed x - point remnant islands are inserted which originate from resonances with q > 3 flux surfaces.

Figure 20 shows the screening due to plasma rotation (for m = 2). Here we note that the analogous curve for m=3 is rather similar to that in Fig.20.

In Figure 21 the screening is a taken into account by reducing the field of the EFCCs according to the screening factor f_s: the ergodized sheath at the boundary stays almost unaffected, whereas

inside the unperturbed separatrix the radial extension of the q = 2 - islands is strongly reduced. An analogous result is obtained for the n = 2 configuration (Fig.22). Here the islands almost disappear. As in Fig. 18 the ergodized region at the x - point contains small islands just outside the q=3 which seem to be more pronounced than in Fig.18. This could increase the transport parallel to the field lines.

8. CONCLUSIONS AND DISCUSSION

The interaction between plasma rotation and the perturbation fields seems to provide the possibility to screen off the perturbation field in the plasma interior and to provide the necessary ergodization at the edge. The experiments and the calculations at TEXTOR and JET show that the rotation level is large enough to avoid the penetration of the external field leading to mode locking. The ergodization of the plasma boundary in TEXTOR is strong enough to generate radial currents leading a significant change of the plasma rotation.

In the case of the EFCCs (n=1) at JET the current I_{hel} is limited at around 35kA (≈75% of the maximum possible current). Increasing the momentum input could extend the window for *Ihel*. The ergodization of the boundary region is in spite of the long distance between plasma edge and the perturbation coils strong enough to mitigate the ELMs.

In fact, the screening in the boundary layer is negligible thus allowing for a good penetration of the field in this region. An improvement should be possible by using the EFCCs in the n=2 configuration because the calculation predict much smaller vacuum islands which are almost removed by the screening effect. The boundary region contains in this case remnant islands which may possible allow a complete ELM - mitigation.

At ITER the main problem is that the momentum transfer from a high energy beam decreases with increasing energy (assuming the same power). Since an energy of 1 MeV is envisaged [46], a decrease of the momentum input by a factor ≈ 3 could lead to a rotation speed considerably lower than in JET . In addition it follows from the global momentum balance that this speed scales inversely with the major radius which is roughly twice as large as that of JET. Since the power at ITER is roughly twice as large than that at JET, the effect of the major radius is presumably compensated.

REFERENCES

[1]. T.E. Stringer, Phys. Rev. Letters, **22**, 770 (1969)

[2]. A. Rogister, Phys. Plasmas, 1, **619**, (1994)

[3]. H.A. Claassen, H. Gerhauser, A. Rogister, C. Yarim, Physics of Plasmas, **7** (2000) 3699

[4]. A. Nicolai, A.L. Rogister, U. Daybelge, Contrib. to Plasma Phys. **42** (2002) 241

[5]. A.L. Rogister, J.E. Rice, A. Nicolai, A. Ince - Cushmann, S. Gangadhara, Alcator C-Mod group, Nucl. Fus. **42** (2002) 1144

[6]. A.L. Rogister, Phys. of Plasmas **6** (1999) 200

[7]. S.J. Braginskii, Transport processes in a plasma, Review of Plasma Physics, New York,

Consultants Bureau, Vol. **1**, (1966) 205

[8]. A. B. Mikhailowski, A. B. Tsypin, V.S., Beitr¨age zur Plasmaphysik, **24** (1984) 335.

[9]. M. Z. Tokar, R. Jaspers, H.R. Koslowski, et al., Plasma Phys. Control. Fusion 41 (1999) B317

[10]. E. Lazzaro, P. Zanca, Phys. Plasmas, Vol. **10** (2003) 2399

[11]. A. Nicolai, U. Daybelge, C. Yarim Nucl. Fus.**44** (2004) S93 - S107

[12]. A. Nicolai, U. Daybelge, C. Yarim Nucl. Fus.**46** (2006) S145 - S153

[13]. A. Nicolai, M. Lehnen, A. Rogister et al. Modelling of Plasma Rotation under the Influence of the Ergodic Dynamic Divertor in the Tokamak TEXTOR, Proceedings of the 13th International Congress on Plasma Physics 2006, Paper B019p

[14]. R. Fitzpatrick, Theory of Fusion Plasmas, Proceedings of the Joint Varenna-Lausanne International Workshop, Varenna (1992), p.147 Phys. Plasmas **2** (1995) 1648

[15]. A. Cole, R. Fitzpatrick, Phys. Plasmas **13** (2006) 032503

[16]. A. Santagiustina, S. A. Arshad, G. Bosia, M. Browns, D. J. Campbell et al., Design of a m=2, n =1 tearing mode control system for JET, Proceedings of the 19th symposium on Fusion Technology (1996) Lisbon, Portugal

[17]. K.H. Finken, G.H. Wolf, B. Giesen, A. Nicolai,M. Haßler, A. Kaleck et al., Special issue on: Dynamic Ergodic Divertor, Fusion Eng. Des. **37** (1997) 341-352

[18]. R.H. Fowler, D. K. Lee, P. W. Gaffney, J. A. Rome, FLOC-Field Line and Orbit Code for the Study of Ripple Beam Injection into Tokamaks, Report ORNL/TM-6293 (1978)

[19]. A. Nicolai, J.Nucl. Mater. **121** (1984) 385

[20]. K. C. Shaing, S. P. Hirshman, J. D. Callen Phys. Fluids **29** (2) (1986) 521

[21]. A.L. Rogister, J. E. Rice, A. Nicolai, P. T. Bonoli, M. J. Greenwald & ALCATOR C-MOD Group, Theory of toroidal plasma rotation in ALCATOR C-MOD ohmic H-mode plasmas, Proceedings of the 28 EPS, paper P3.034, 2001

[22]. R. Jaspers, private communication, FZ Jülich (2002)

[23]. J.E. Rice, J. A. Goetz, R.S. Granetz, M.J. Greenwald, A.E. Hubbard et al., Phys. Plasmas 7 (2000) 1825

[24]. J. E. Rice, W. D. Lee, E. S. Marmar, N. P. Basse et al, Physics of Plasmas, **11** (2004) 2427

[25]. A. Bortolon, B.P.Duval, A. Pochelon, A. Scarabosio, Phys Rev. Lett., **97**, (2006) 235003

[26]. T. E. Evans, R. A. Moyer, P. R, Thomas, J. G. Watkins et al., Phys . Rev. Lett., 92 (2004) 235003-1

[27]. V. Parail, T. Evans, T. Johnson, N.Oyama et al. Theoretical analysis and predictive modelling of ELMs mitigation by enhanced toroidal ripple and ergodic magnetic field, 21st IAEA Fusion Energy Conference, Chengdu (2006) paper TH/P8-5

[28]. M. Becoulet, E. Nardon, G. Huysmans, P. Thomas, Modelling of Edge Control by Ergodic Fields in DIII-D, JET and ITER, 21st IAEA Fusion Energy Conference, Chengdu (2006) paper TH/P1 - 29

[29]. J. Wesson, Tokamaks, Clarendon Press - Oxford (1997)
[30]. R. Singh, private communication, 2005
[31]. C. Gourdon, Report IPP P12 483, Garching, Oktober 1970 (translated by J.Eisert)
[32]. M. Coronado, H. Wobig, Phys. Fluids **29** (1988) 527
[33]. K. Audenaerde, G.A. Emmert, and M. Gordinier, University of Wisconsin, Report UWFDM-259, 1978
[34]. S. T. Hahm, K. H. Burrell Phys. Plasmas **2** (1995) 1648
[35]. R. H. Fowler, J. A. Rome Report ORNL 6845 (1975)
[36]. A. Nicolai et al. Journal of Computational Physics, Vol. 80 (1989) 98
[37]. V. K. Mel'nikov, Soviet Physics - Doklady **7** (1962) 502
[38]. A. Nicolai, U. Daybelge. C. Yarim, Theory of Fusion Plasmas, Proceedings of the Joint Varenna-Lausanne International Workshop, Varenna (2004), p.381
[39]. A. Nicolai, U. Daybelge. M. Lehnen, A. Rogister, M.Tokar, B. Unterberg, R.C.Wolf, C. Yarim,Modelling of Plasma Rotation under the Influence of the Ergodic Dynamic Divertor in the Tokamak TEXTOR, Proceedings of the 13th Intenational Congress on Plasma Physics, Kiev, 2006, Paper B011p.
[40]. M. Lehnen, S.S.Abdullaev, W. Biel, M.F.M. de Bock et al., Plasma Physics and Controlled Fusion 94 (2005) 015003
[41]. I. Kaganovich, V. Rozhansky, Phys. Plasmas **5** (1998) 3901 Plas. 6 (1999) 153
[42]. M. Tokar, Krakau
[43]. T.E. Evans, R.A. Moyer, K. H. Burell et al. Nature Physics, **2** (2006) 419
[44]. Y. Liang, H.R. Koslowski, P. R. Thomas, E. Nardon at al. submitted to PRL (226)
[45]. C.G. Gimblett, private communication (2007)
[46]. P.L. Mondino, P.Bayetti, E. di Pietro, R. Hemsworth et al., Iter Neutral Beam System, Report ITERP1/17

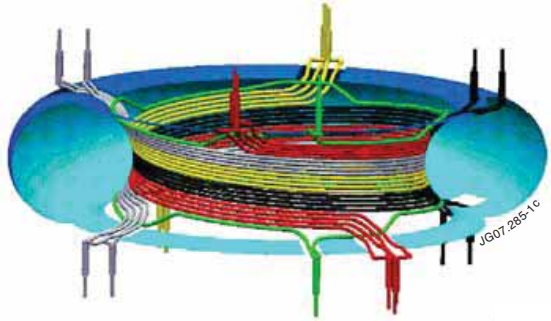

Figure 1: The Dynamic Ergodic Divertor (DED) at TEXTOR has helical windings which are roughly parallel to the field lines in the q=3 surface. Here the winding is switched in the m=3 and n=1 configuration

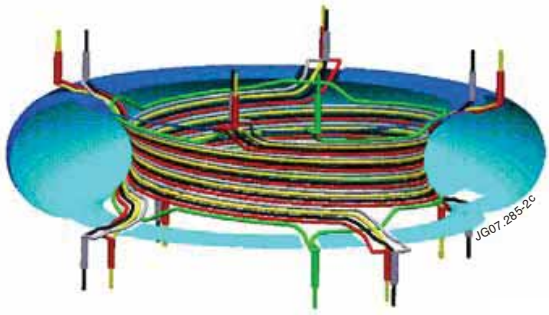

Figure 2: The DED can be switched to the m=12, n=4 configuration, where two neighboring conductors the opposite current direction. This is the configuration with the highest m and n

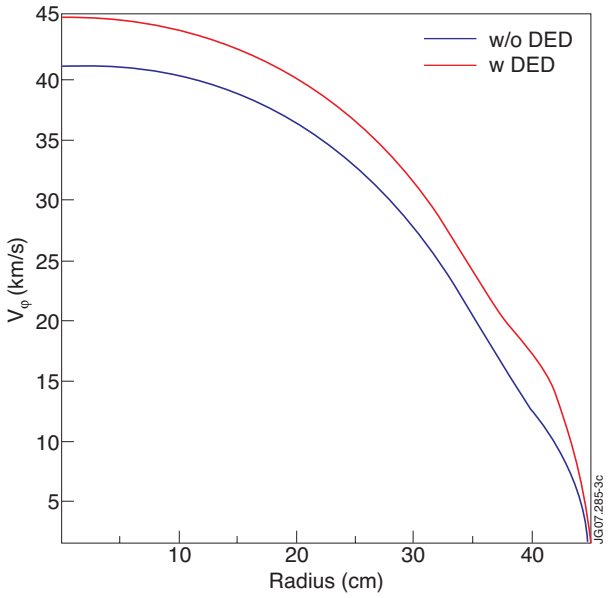

Figure 3: In the case of co-injection the ergodic momentum input (P_{NBI}=0.35MW) increases the toroidal velocity by 5 km/sec in the boundary region. Except for this region the gradient of the profile stays unchanged.

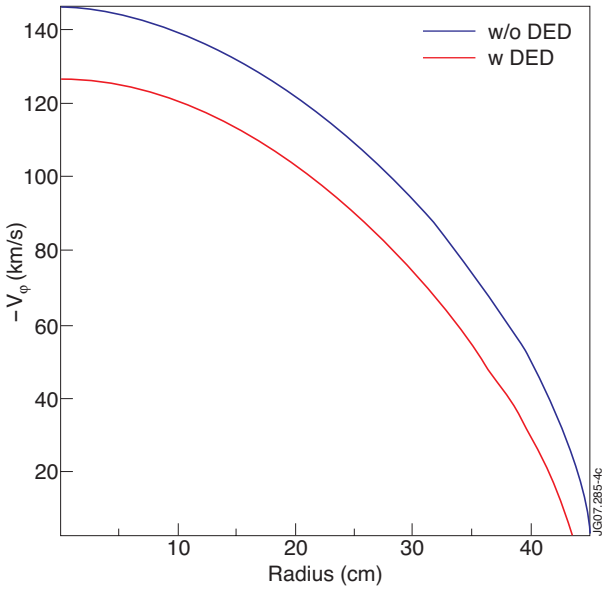

Figure 4: In the case of counter - injection the ergodic momentum (P_{NBI} =1.3MW) input decreases the toroidal velocity by 20 km/sec in the boundary region . Except for this region the gradient of the profile stays unchanged as in Fig.3. The sign of the ergodic momentum input is the same as in Fig.3.

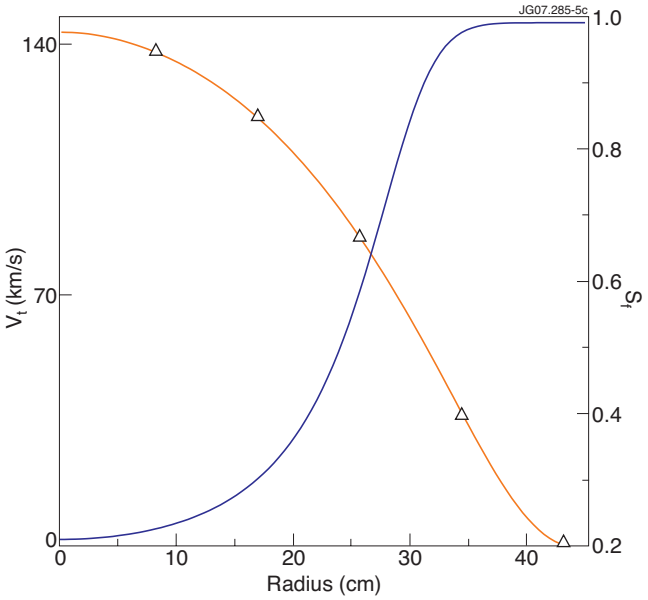

Figure 5: Toroidal velocity and screening for Pulse No: 97613 The ponderomotive forces are well screened in the plasma interior.

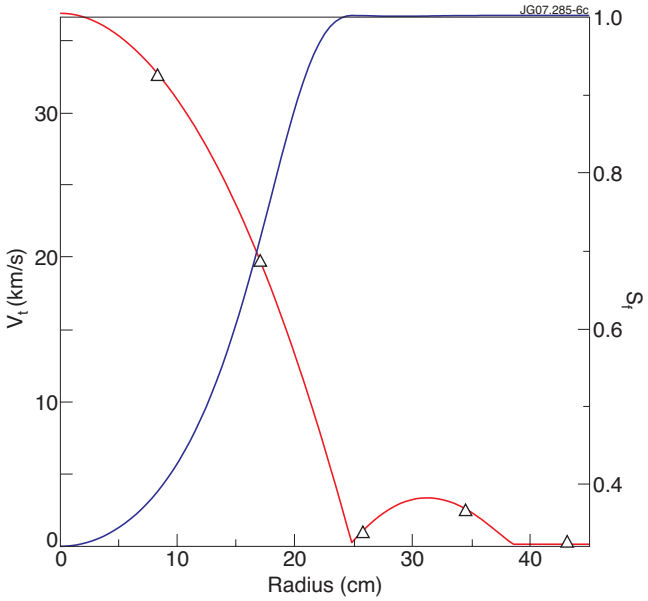

Figure 6: The braked solution demonstrates the action of the ponderomotive force at the q = 2 surface. This solution is obtained for IDED > 2kA.

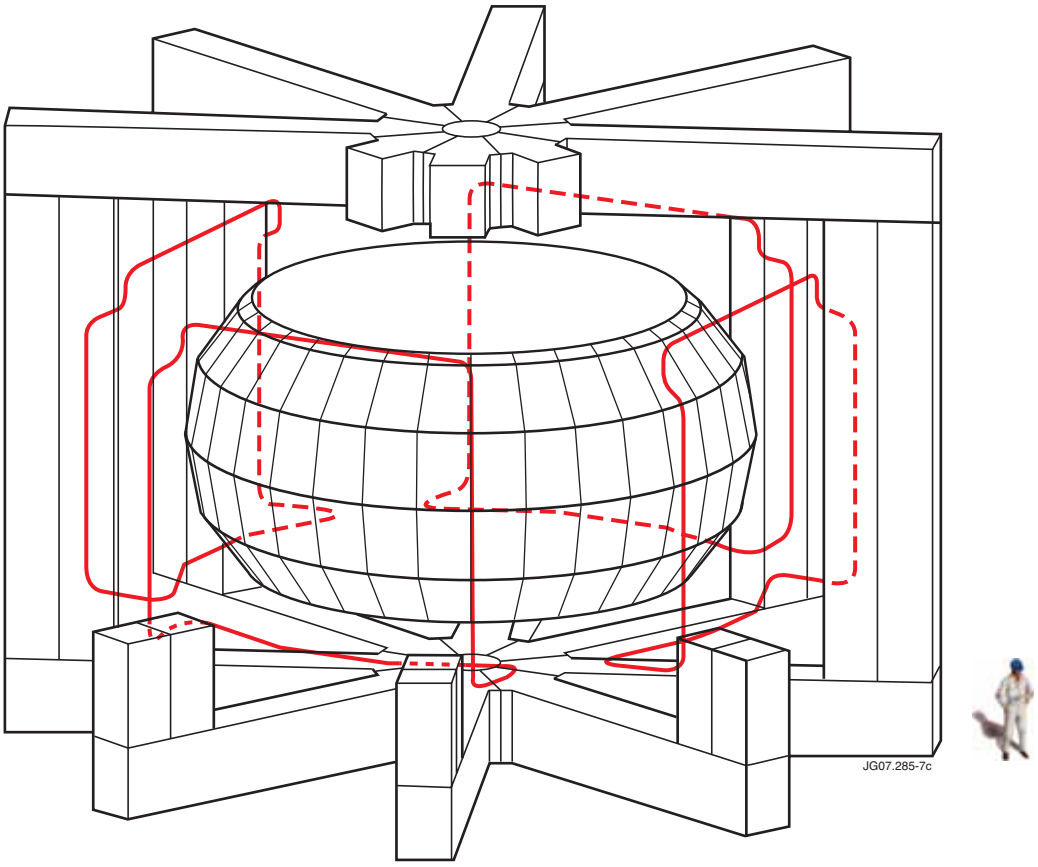

Figure 7: The Error Field Correction Coils (EFCCs) are mounted at the outer limbs of the yokes. The toroidal extension of one coil is 70^o and the shape is approximately that of square with a side length of ≈ 6m. The maximum distance of the conductors from the axis of symmetry is 7m. The maximum current in each coil (with 3 turns) is 48 kA, i.e. 16kA per turn.

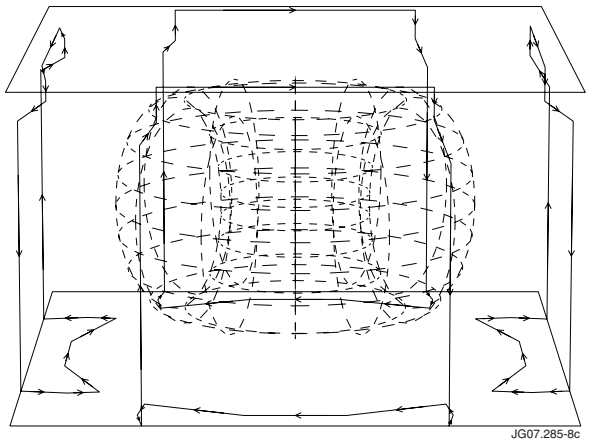

Figure 8: EFCC's configured for n=1 where two neighboring coils are switched in parallel and the two opposite coils have both the opposite current direction

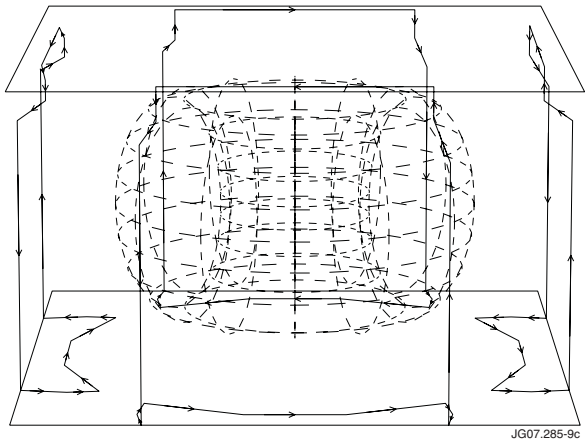

Figure 9: EFCC's configured for n=2 where two neighboring coils have the opposite current direction

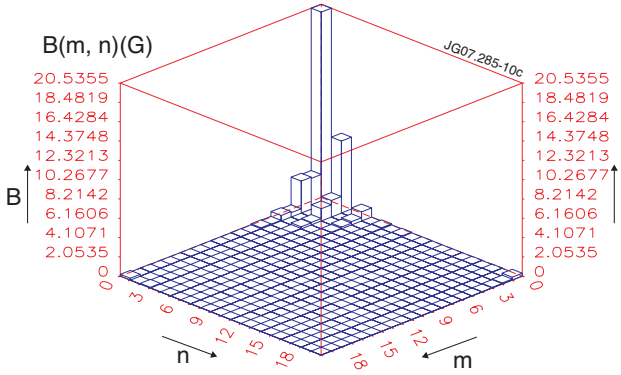

Figure 10: Spectrum for the n=1 configuration. The (m=1, n=1) component is the largest because of the good overlap with sin(θ – ϕ). The (m=2, n=1) component is comparable to the (m=1, n=3) component and both are around one half of the (m=1, n=1) component.

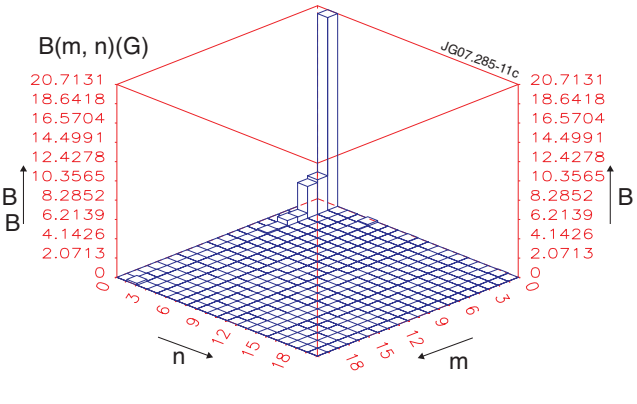

Figure 11: The analogous spectrum for the n=2 configuration. The (m=1, n=2) component is the largest component, followed by the the (m=2, n=2) component.

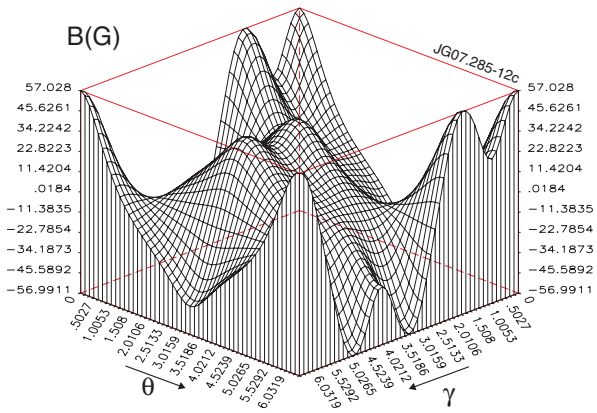

Figure 12: The radial field of the n=1 - coil configuration (Fig. 8) at the θ = 3 surface. For θ = 0 the dependence $B_r \approx \sin(\phi)$ can be seen which is the main reason for the large $B_{1,1}$ - component in Fig.10. Also the modulation by the B3,1- component is evident in accordance with Fig.10.

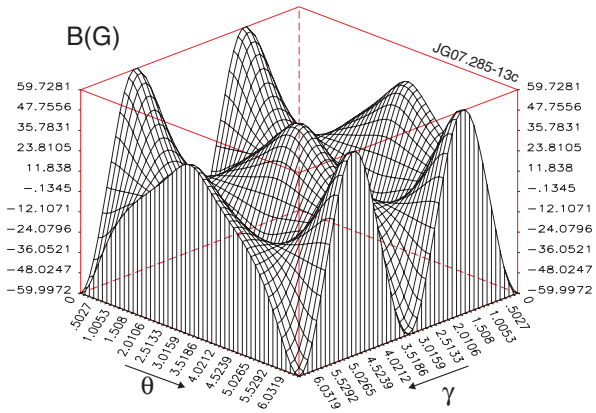

Figure 13: The radial field of the n=2 - coil configuration (Fig.9) at the q=3 surface. For θ = 0 the dependence $B_r \approx \sin(2\phi - {}^{\pi}/_{2})$ can be seen which is the main reason for the large B2,1 component in Fig.11. Since the coils have the 'natural' mode number n=2 almost no modulation of of the aforementioned dependence can be seen.

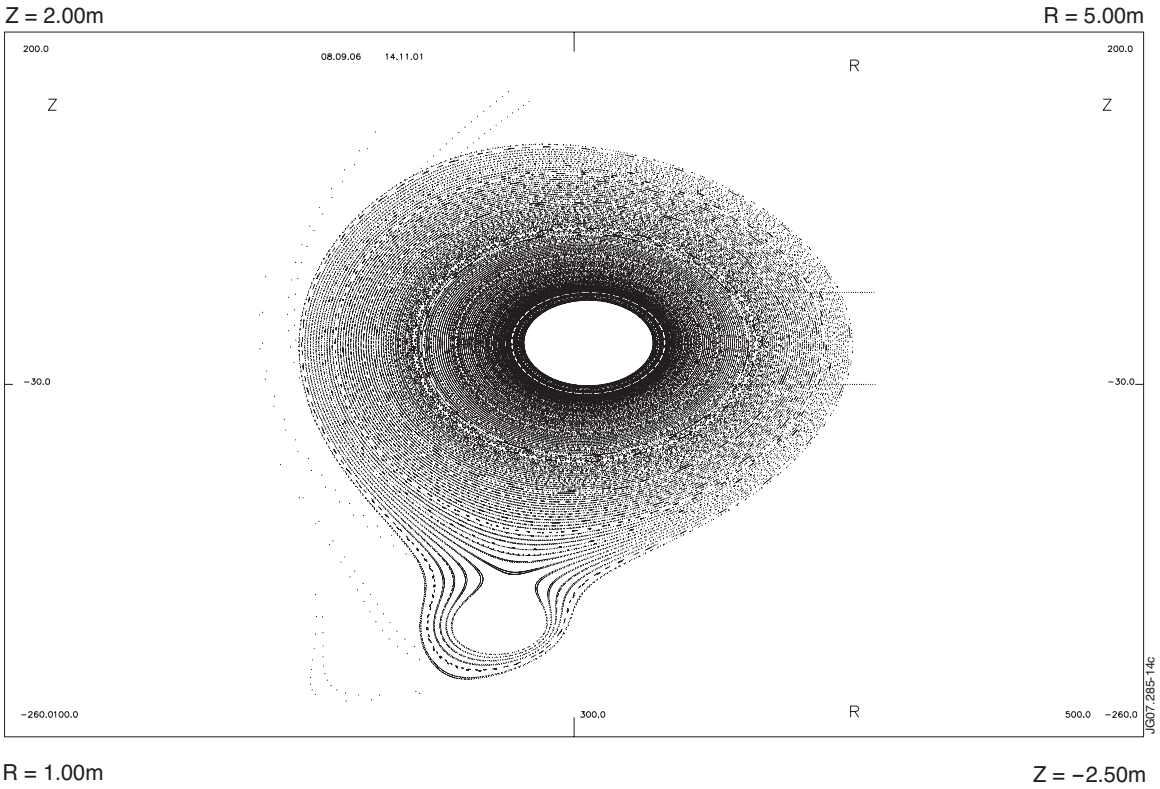

Figure 14: Unperturbed configuration; Since mainly the x-point region is of interest here, one divertor coil was assumed below the elliptical and triangular plasma with JET - dimensions (R_0 = 296cm, a=85cm, δ = 0.3 ,r_{max} = 120cm).

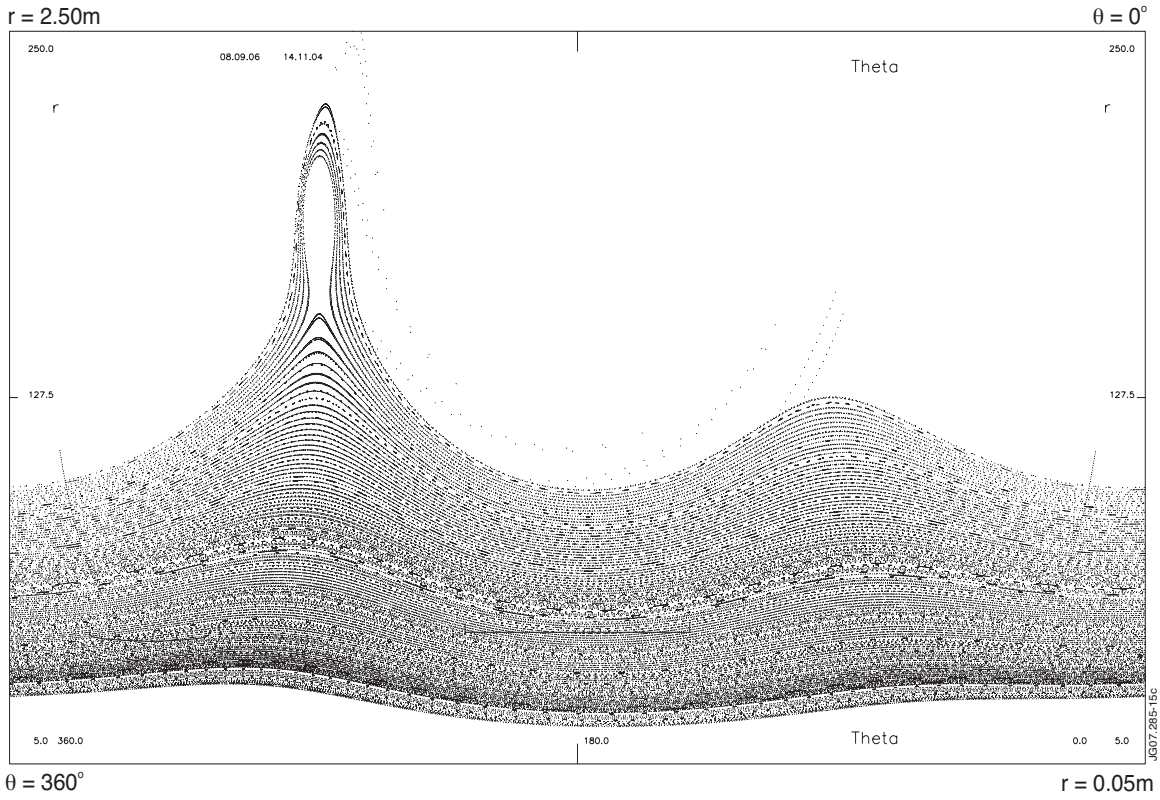

Figure 15: The configuration as in the Fig. before using the (r, θ) representation.

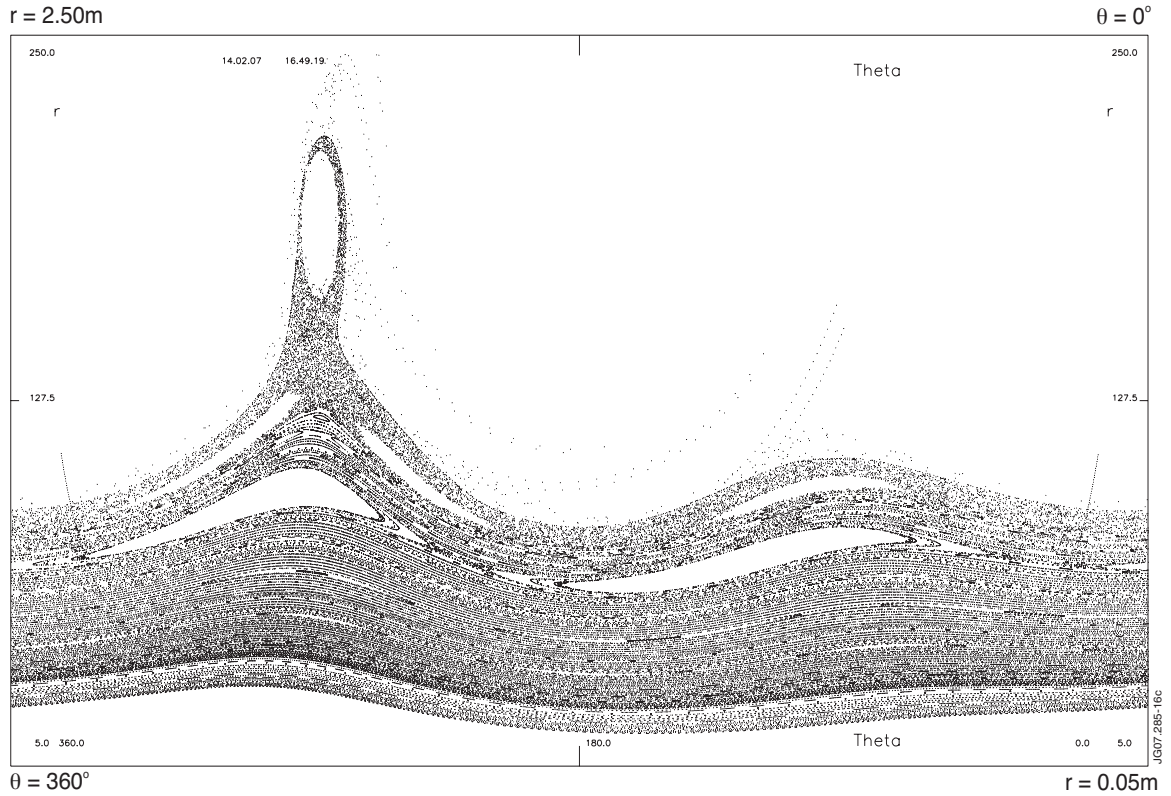

Figure 16: The Poincaré plot generated by the n=1 configuration in (Fig.8) is consistent with the spectrum (Fig.11). As expected, the n=1 configuration generates pronounced islands at the q=2 and q=3 surface. The ergodization of the separatrix region is clearly visible; at the x-point the thickness of the ergodized layer is around 20cm.

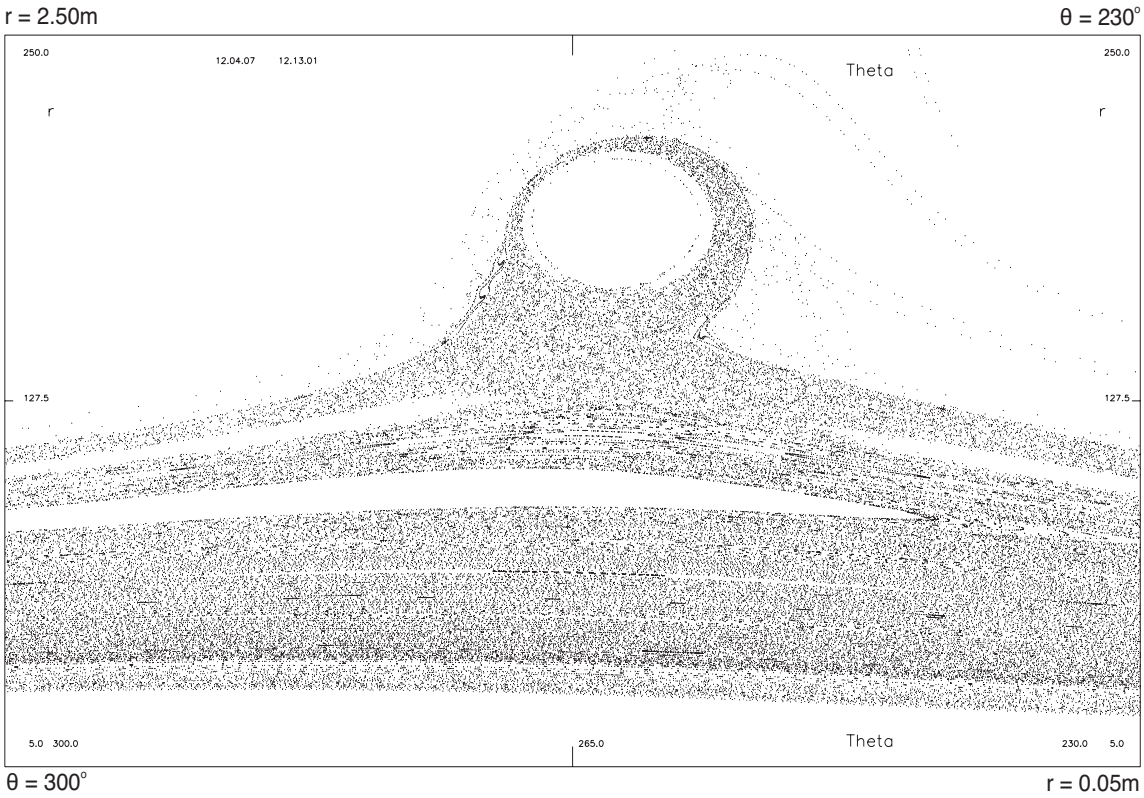

Figure 17. The Poincaré plot generated by the n=1 configuration in (Fig.8) for theenvironment of the x - point in the poloidal range [230°-300°]. The number of initial points hade been doubled to in crease the mean density of the intersection points with ϕ =0. The ergodic region around the unperturbed x - point does not contain remnat island in contrast to Fig. 19.

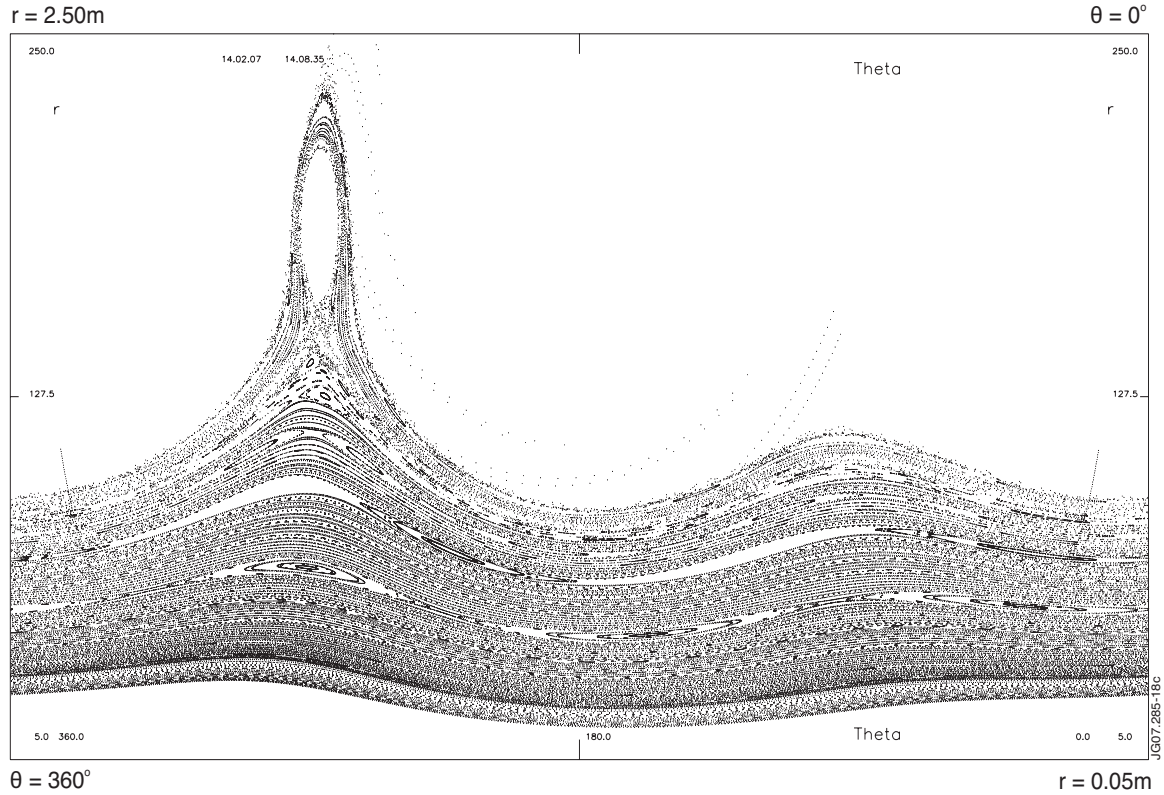

Figure 18: The Poincaré plot generated by the n=2 configuration in (Fig.9) is consistent with the spectrum (Fig.11) as well. The (m=3, n=2) and (m=4, n=2) island chains are visible but the island widths are rather small.

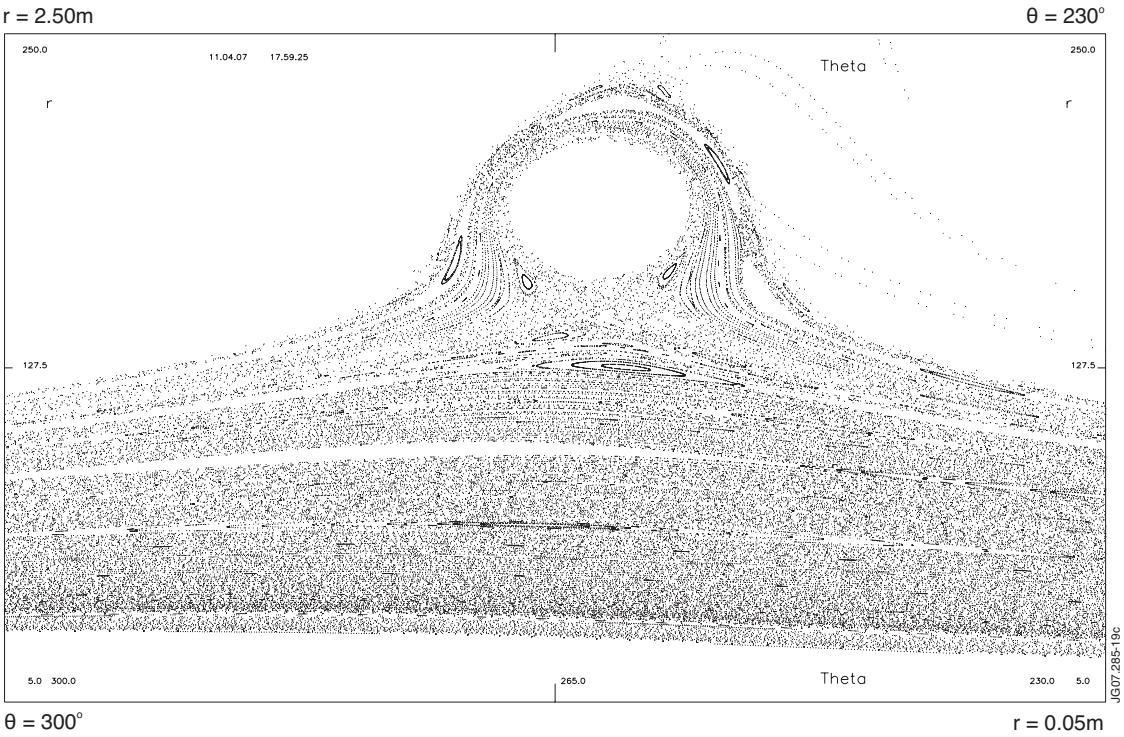

Figure 19: The Poincaré plot generated by the n=2 configuration in (Fig.9) for the environment of the x - point in the poloidal range [230°–300°]. The number of initial points have been doubled to in crease the mean density of the intersection points with $\phi = 0$. Remnant island are inserted in the ergodic region around the unperturbed x - point. This region seems to be somewhat smaller than in Fig.17.

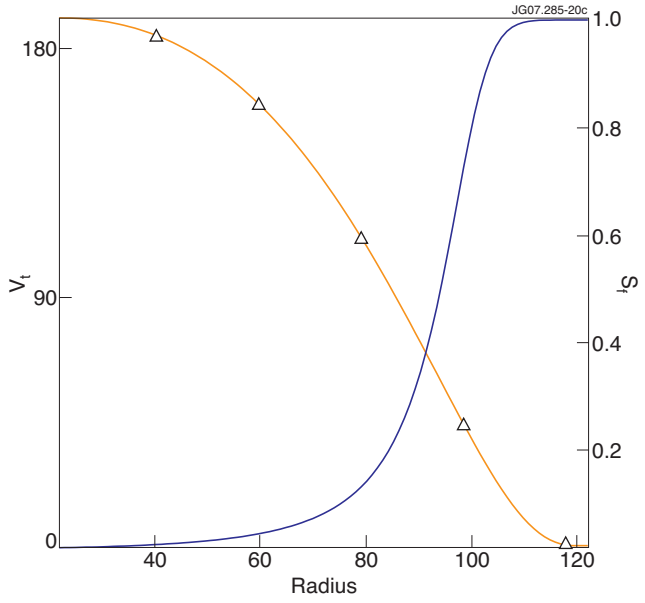

Figure 20: The toroidal plasmarotation effects at the beginning of the current rise in the EFCC - coils a screening factor which is very small in the plasma interior.

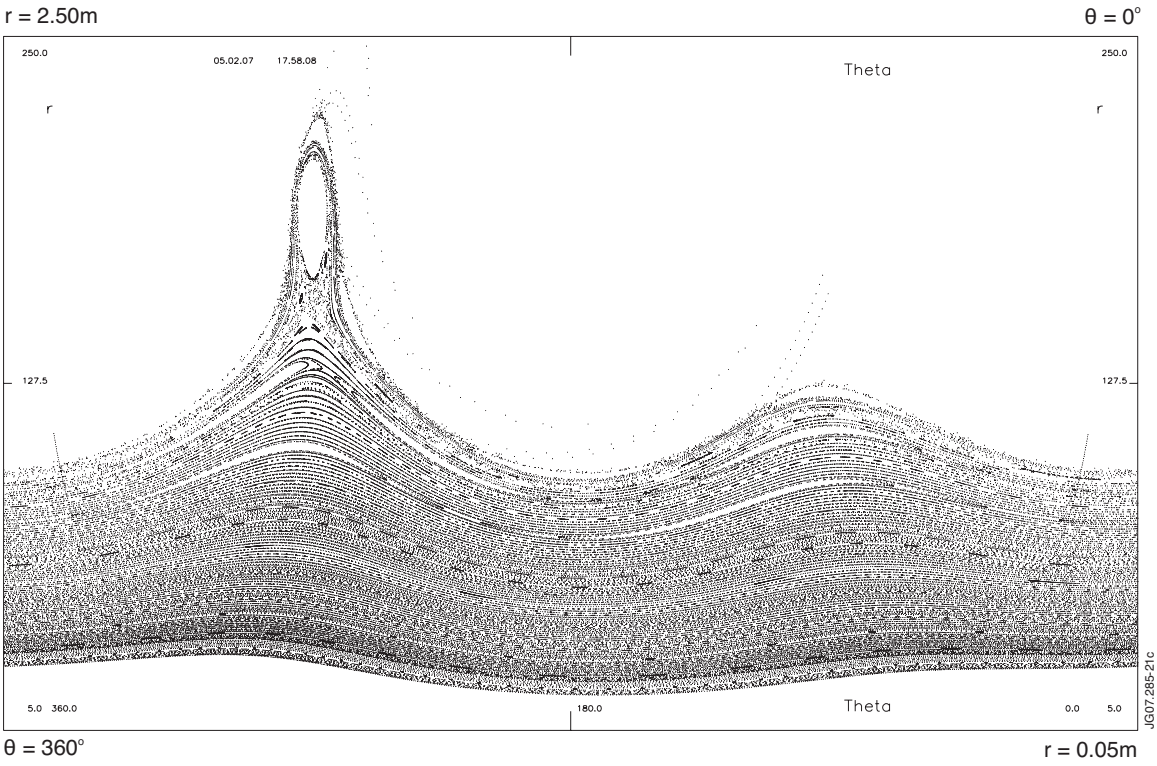

Figure 21: The screening effects a strong reduction of the island size but does not remove it mainly because the island width is proportional to $\sqrt{B_r/B_0}$, $(B_r/B_0 << 1)$

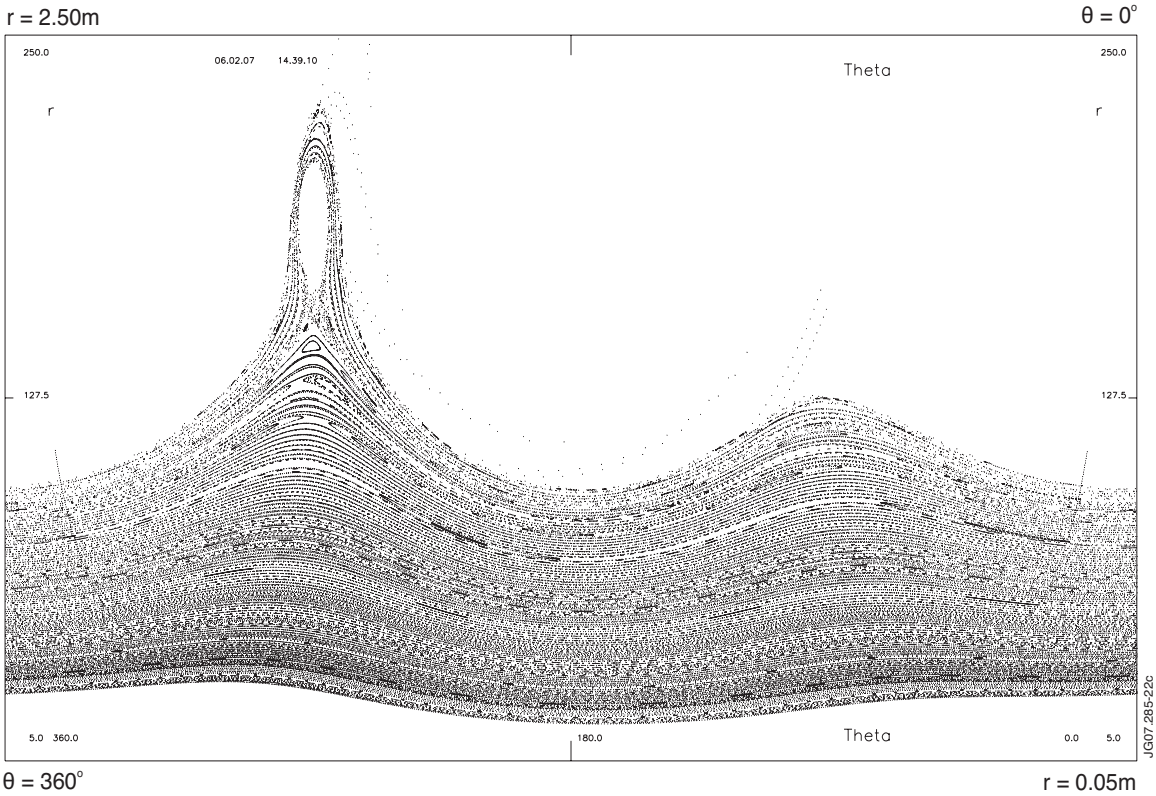

Figure 22: As in Fig. 21 the screening effects a reduction of the island size and removes it almost.